



Electrochemically Deposited Tin-Silver-Copper Ternary Solder Alloys

Bioh Kim*^z and Tom Ritzdorf*

Semitool, Incorporated, ECD Division, Kalispell, Montana, 59901, USA

A study on film properties of electrochemically deposited tin-silver-copper (SnAgCu) alloys was performed with an alkaline bath. This research focused on the bath and process development for dendrite-free, near-eutectic SnAgCu alloy deposition through the investigation of cathodic polarization, morphological transition, and film composition. Effects of process parameters on surface morphology, film composition, and diffusion-limited current density (LCD) were also examined. Ternary alloys were obtained only when the current density was driven beyond the mass-transfer limitation of noble metals (silver and copper), which seemed to cause the transition of surface morphology and film composition with increasing current density. The morphological transition occurred through four stages (dendrites, suppression of dendrites, nodules, and columns/dendrites), and the content of noble metals in the film tended to drop with increasing current density. With increasing the concentration of noble metals, bath temperature, and agitation, the morphology at low current densities became increasingly dendrite-dominated and the content of noble metals in the film was enhanced at a fixed current density. The morphology of stage four was influenced by the ratio of the applied current density to the LCD, where the LCD was significantly influenced by the metal concentration, bath temperature, and agitation.
© 2002 The Electrochemical Society. [DOI: 10.1149/1.1530153] All rights reserved.

Manuscript submitted January 9, 2002; revised manuscript received July 23 2002. Available electronically December 23, 2002.

Mounting is a critical step in semiconductor-related device manufacture. With the electronic devices miniaturized and the circuitry complicated, the mounting of a microelectronic substrate to another substrate becomes more and more difficult. Therefore, interconnection techniques with high density, performance, and reliability are desirable for microelectronic substrates. Flip chip technology, which involves turning over a chip and then bonding the terminals directly to a wiring substrate, is used instead of conventional mounting technologies such as wire bonding or tape automated bonding. The advantages of this technology include high-density bonding, gang bonding, improved electrical performance, self-alignment, reliability and manufacturability.^{1,2}

The most widely used solders for flip chip applications are based on lead-tin alloys. However, there is currently substantial interest in looking for lead-free solder alloys because of legislation due to the toxicity of lead.³ Another concern for upcoming technology generations is soft error generation caused by lead in flip-chip solder connections. This is due to alpha particle emission from the lead.⁴ Tin-silver and tin-silver-based alloys are being developed to use as lead-free solder bumps.⁵⁻¹⁰

Near-eutectic SnAgCu alloys are receiving a growing interest due to such merits as good melting, solderability, ability to cope with lead contamination, and reliability.^{11,12} To use these alloys for general purpose solders, the contents of silver and copper in alloys are limited to near-eutectic compositions (3.4-4.1 wt % Ag and 0.45-0.9 wt % Cu) on account of the limited level of melting points for bumping applications.¹² SnAgCu alloys are being investigated as alternatives to lead-bearing alloys for solder bumps, but the mainstream method of formation has been limited to screen printing technology, because this is a low-cost method for producing relatively large geometry bumps.¹³⁻¹⁹ However, this method has serious limitation as the size/pitch of solder bumps decreases. As the density of patterns and the complexity of circuitry increase, electrodeposition technology becomes preferred as an alternative method to screen printing.²⁰

The purpose of this study was to develop a bath and process that could produce dendrite-free, near-eutectic SnAgCu alloys for lead-free bumping applications. Within this study, several process conditions using an alkaline bath were tested and their influences were measured. For example, the cathodic polarization tests of a new bath were conducted, surface morphology and film composition were investigated with varying current densities, and the relationship

among polarization, surface morphology, and film composition was discussed. Effects of process parameters on surface morphology, film composition, and diffusion-limited current density (LCD) were also examined.

Experimental

Wafers.—Wafers for testing cathodic polarization had the structure of Si(substrate)/SiO₂/TiN (40 nm)/Pt (50 nm). Platinum seed layer was sputter-deposited. Wafers for characterizing surface morphology, film composition, and LCD had the structure of Si (substrate)/SiO₂/Ta (25 nm)/Cu (100 nm)/Cu (5 μm). A thin copper layer was sputter-deposited, whereas the thick copper layer was electrochemically deposited.

Cathodic polarization.—In order to mount the wafers in a conventional rotating disk electrode (RDE) with as little hydrodynamic disturbance as possible, a device was manufactured which is referred to as the modified rotating disk electrode (MRDE) and is illustrated in Fig. 1.²¹ To use this MRDE, the wafer was sectioned into 1.5 × 1.5 cm pieces and the wafer piece was then mounted to the MRDE. The result was that no conducting part except for the exposed wafer with a 1.2 cm diam came into contact with the plating solution. Additional characterization of the bath was performed using an EG&G platinum RDE with a 4 mm diam. The MRDE and

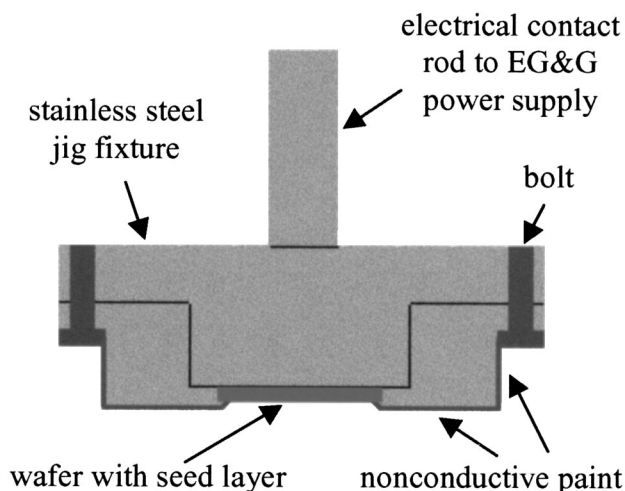


Figure 1. Schematic drawing of MRDE.

* Electrochemical Society Active Member.

^z E-mail: bkim@semitool.com

Table I. Summary of process conditions used for experiments.

Parameters		Conditions		
Bath concentration (mol/L)	Bath type	Sn	Ag	Cu
	1	0.500	0.008	0.004
	2	0.500	0.012	0.004
	3	0.500	0.012	0.006
	4	0.500	0.024	0.012
	5	0.750	0.012	0.006
	6	0.400	0.010	0.010
7	0.400	0.005	0.005	
Temperature (°C)	20, 30, 40, and 50 (± 0.5)			
Agitation (rpm)	0, 100, and 200 (± 10)			
pH	7.5, 8.5, and 9.5 (± 0.2)			

RDE were rotated at the desired rpm using an EG&G model 616 RDE motor. The potentiostat used for linear scans was the EG&G model 263A with EG&G 270 electrochemical software. The scan rate was 20 mV/s. An Ag/AgCl reference electrode was used and the measured potential was converted to standard hydrogen electrode (SHE).

Surface morphology, film composition, and LCD.—To evaluate film properties, wafer segments with an area of approximately 3.0 cm² were used as a cathode and a large area of platinized-titanium sheet was used as an anode. Experiments were performed in a 1.5 L beaker containing 1 L of plating solution. The power supply used for these experiments was an HP model E3617E DC. The deposition time for each current density was adjusted to meet the target thickness (10 μm). For example, it took 25 min to deposit a 10 μm thick film with a current density of 10 mA/cm² (at room temperature and no agitation). This rate was used as a reference value to set up the deposition time for different current densities. Tested process conditions including bath concentrations are listed in Table I. Each bath was composed of tin ions, silver ions, copper ions, and two complexing agents. Complexing agents were used to shift the reduction potential of noble metal ions (silver and copper) to more cathodic values by forming ion complexes. A scanning electron microscope (SEM, AMRAY model 3600 FE SEM) and an energy-dispersive spectrometer (EDS, Noran Voyager) were used to observe surface morphology and examine film composition, respectively. Film thickness was measured with a Veeco surface metrology tool (Dektak 300-Si). Chronopotentiometric data were obtained with the same potentiostat in order to evaluate the LCD of ternary alloy deposition.

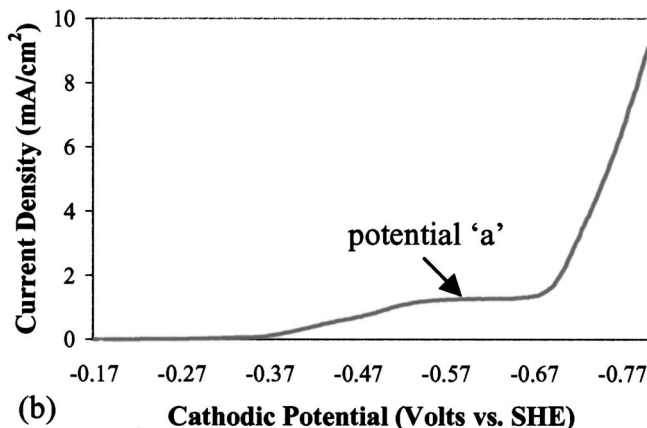
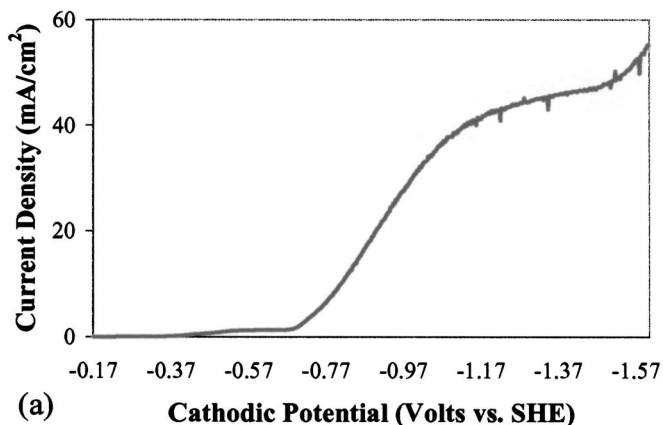


Figure 2. (a) Cathodic polarization curve of SnAgCu bath showing two plateaus, one by the mass-transfer limitation of noble metals and the other by that of tin and (b) initial parts showing first plateau and deposition potential “a” used for potentiostatic deposition. 20 mV/s scan rate, bath 6 (0.4 mol/L Sn, 0.01 mol/L Ag, and 0.01 mol/L Cu), room temperature, 100 rpm, and pH 9.5.

Results and Discussion

Cathodic polarization, morphological transition, and film composition.—A cyanide-free, alkaline bath was developed for electrochemically depositing ternary SnAgCu solder alloys. As the contents of silver and copper in these alloys for bumping applications

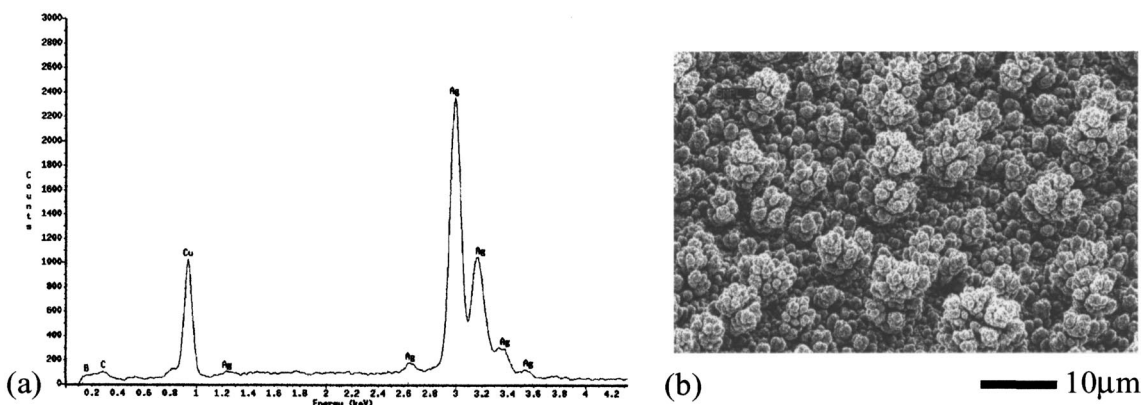


Figure 3. (a) EDS spectrum (average composition in wt %: 56 Ag-44 Cu) and (b) surface morphology of deposit obtained at potential “a”. Bath 6 (0.4 mol/L Sn, 0.01 mol/L Ag, and 0.01 mol/L Cu), room temperature, 100 rpm, and pH 9.5.

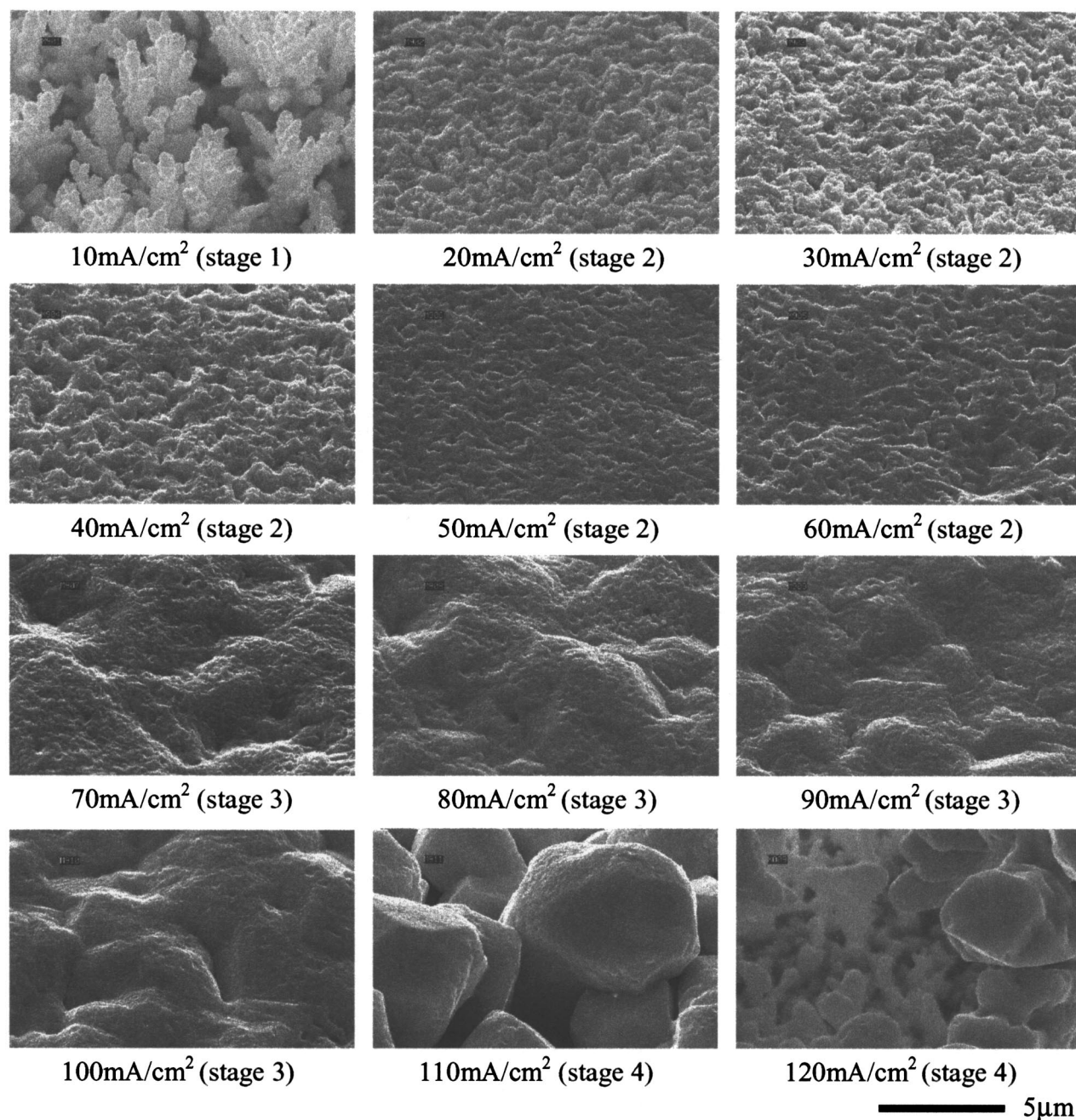


Figure 4. Morphological transition with increasing current density. Electric charge density of 18 C/cm^2 at each current density, bath 5 (0.75 mol/L Sn, 0.012 mol/L Ag, and 0.006 mol/L Cu), 40°C , 200 rpm, and pH 9.5.

are very low (generally, $<4.1 \text{ wt } \% \text{ Ag}$ and $<0.9 \text{ wt } \% \text{ Cu}$),¹² the bath also contains small amounts of silver and copper. Baths used for these experiments are listed in Table I. These baths did not show any precipitation or color change for more than 6 months without applying current.

Polarization tests were conducted with an MRDE to characterize the surface morphology and film composition of deposits obtained at each potential. Experiments were performed with bath 6 at room temperature, 100 rpm, and pH 9.5. The result is illustrated in Fig. 2a. The initial part that was gently sloping and then forming a plateau, shown in Fig. 2b, corresponds to the potentials at which primarily the binary silver-copper alloys are deposited. As shown in Fig. 3a, the deposit obtained potentiostatically from the deposition potential a in Fig. 2b was a binary alloy composed of 56 wt % Ag and 44 wt % Cu. No tin was observed in this alloy, as can be seen from the

EDS spectrum. It was found from more studies that the composition of binary alloys varied with changing potential due to the difference of deposition potential between silver and copper in the bath. The deposit was very dendritic as seen in Fig. 3b, and there was no change of induced current density in a wide range of potential as seen in Fig. 2b. It can be deduced from these results that the first plateau comes from the mass-transfer limitation of noble metal ions and that ternary alloys are obtained only when the current density is driven beyond the mass-transfer limitation of noble metals. Driving current density beyond this point causes the voltage to increase to a point where tin is codeposited, leading to ternary alloy deposition. At a potential of approximately -0.7 V , the curve begins to rise sharply until it reaches the potential where the mass-transfer limitation of tin ions occurs. This rise is related to the inclusion of the tin in the deposit, as mentioned previously. Therefore, ternary alloys

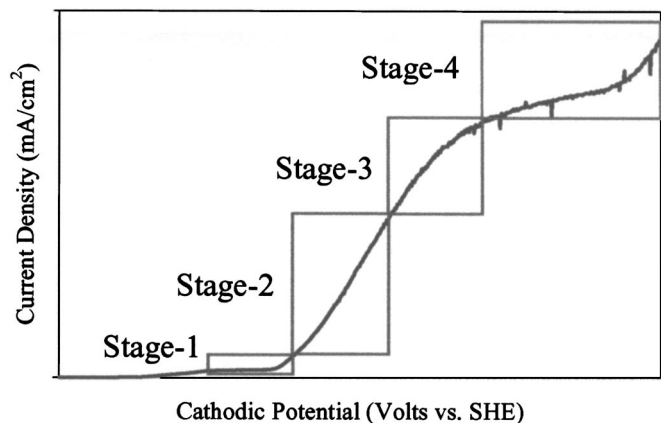


Figure 5. Approximated relationship between polarization curve and surface morphology.

can be obtained from this potential. Another rise at about -1.5 V after the second plateau results from proton discharge (hydrogen gas evolution). After the polarization tests were completed, electrodeposition runs were conducted at various current densities in order to investigate the transition of surface morphology and film composition with varying current densities.

The morphological transition of ternary alloys with increasing current density was examined and is shown in Fig. 4. The morphological transition of deposits occurred through four stages with increasing current density; dendritic growth (stage 1), suppression of dendrites (stage 2), nodular growth (stage 3), and columnar/dendritic growth (stage 4). The following can be considered as the driving force for the morphological transition with increasing current density. Stage 1 seems to result from the mass-transfer limitation of silver and copper as seen from Fig. 3, where the ternary alloy deposition occurs at a current density higher than the formation of the dendritic, binary silver-copper alloys. Up to a certain potential after the first plateau, the initial, ternary alloys containing high amounts of noble metals can also be under the influence of the mass-transfer limitation of noble metals. In other words, the low concentration of noble metals in the bath can be the source of dendrites. Because of the higher (less cathodic) reduction potential of silver and copper relative to tin, these ions tend to be preferentially deposited at low potentials. However, the supply of these ions to the surface is very limited, resulting in dendrites at low potentials. Tin is deposited preferentially with an increase in current density, suppressing den-

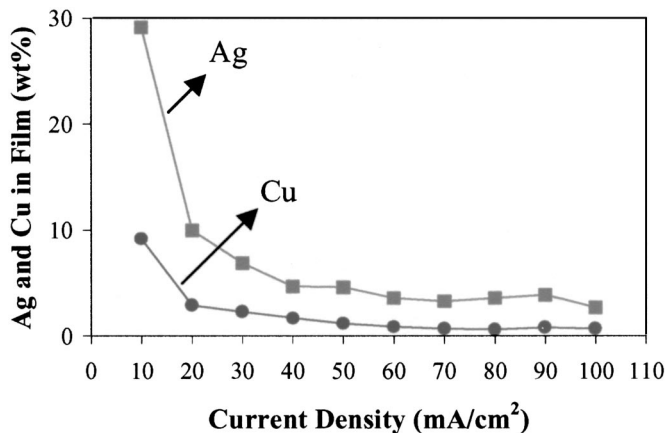
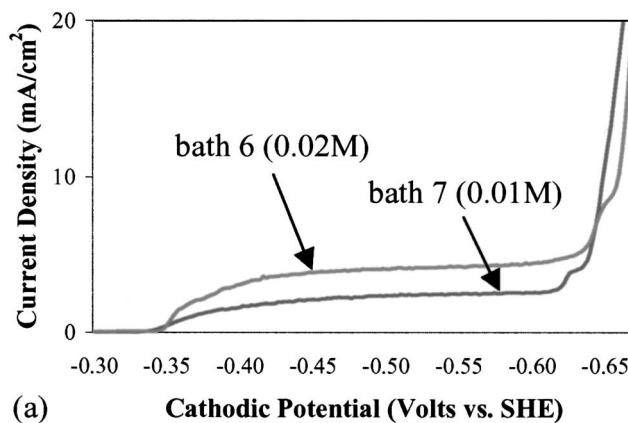
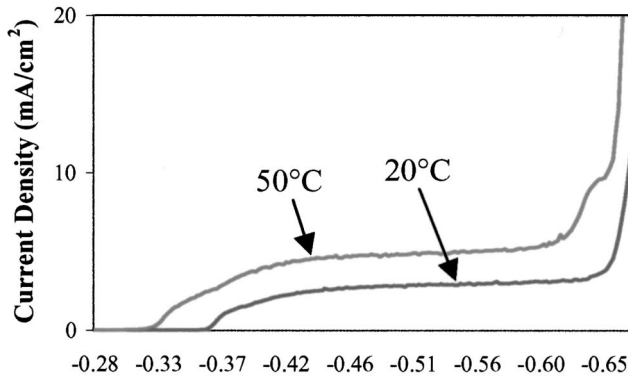


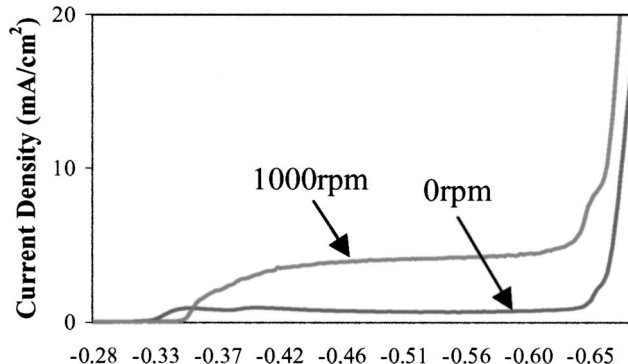
Figure 6. The change of film composition with increasing current density. Bath 5 (0.75 mol/L Sn, 0.012 mol/L Ag, and 0.006 mol/L Cu), 40°C , 200 rpm, and pH 9.5.



(a) Cathodic Potential (Volts vs. SHE)



(b) Cathodic Potential (Volts vs. SHE)



(c) Cathodic Potential (Volts vs. SHE)

Figure 7. Effects of process parameters on the noble metal LCD (first plateau). (a) Effect of the concentration of noble metals. 20 mV/s scan rate, bath 6 (0.4 mol/L Sn, 0.01 mol/L Ag, and 0.01 mol/L Cu) and bath 7 (0.4 mol/L Sn, 0.005 mol/L Ag, and 0.005 mol/L Cu), 1000 rpm, room temperature, and pH 9.5. (b) Effect of bath temperature: 20 mV/s scan rate, bath 7 (0.4 mol/L Sn, 0.005 mol/L Ag, and 0.005 mol/L Cu), 1000 rpm, and pH 9.5. (c) Effect of agitation. 20 mV/s scan rate, bath 6 (0.4 mol/L Sn, 0.01 mol/L Ag, and 0.01 mol/L Cu), room temperature, and pH 9.5.

drites induced by the mass-transfer limitation of noble metals (stage 2). In this case, the transition seems to occur between 10 and 20 mA/cm². Fully suppressed, smooth surfaces were obtained between 60 and 70 mA/cm². Deposits were transformed to stage 3 (development of nodules) with further increasing current density, where the mechanism of deposition is thought to change from charge-transfer control to mixed control, resulting in secondary, nodular growth. The topography of stage 3 morphology was enhanced with increasing current density. Under mass-transfer control

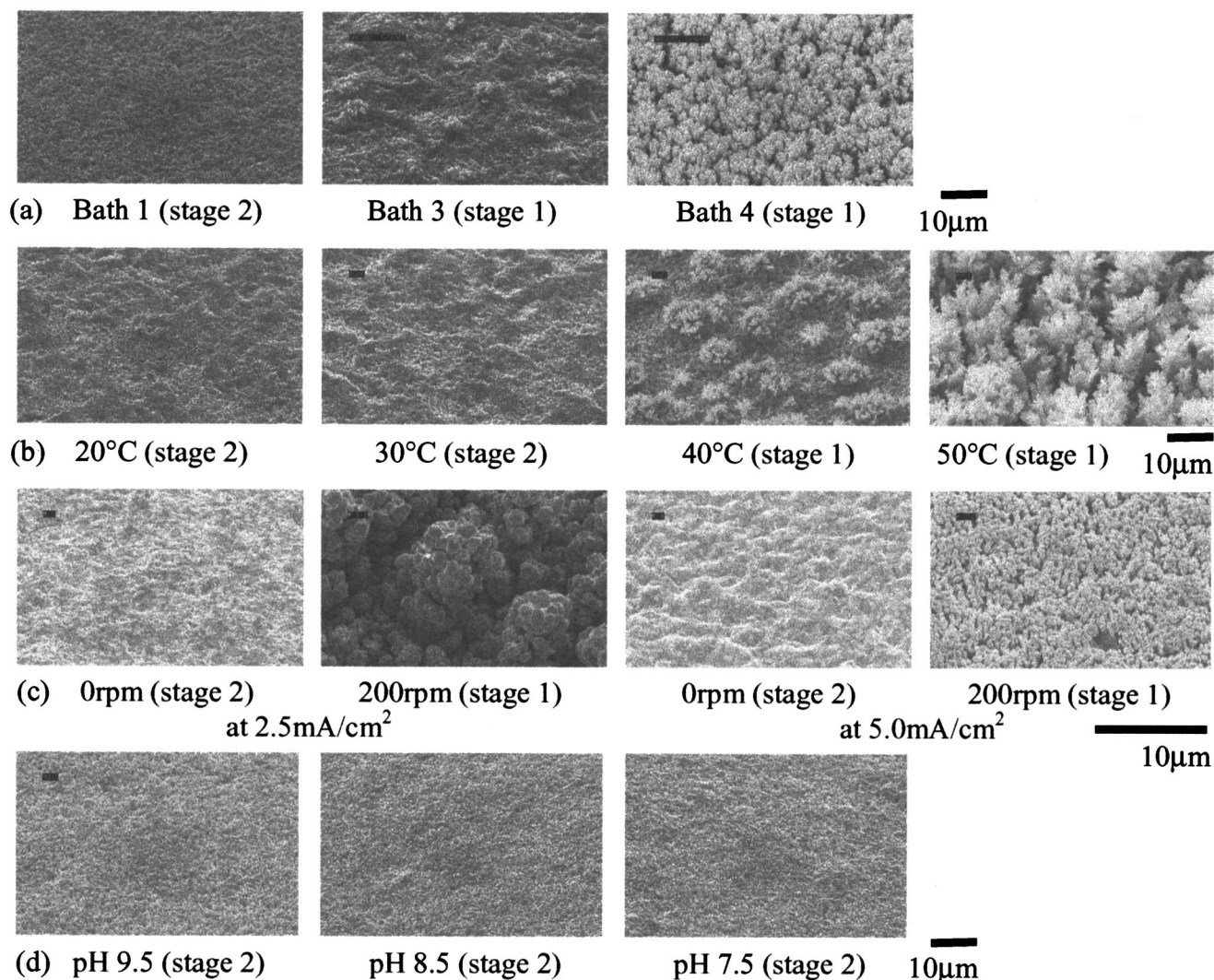


Figure 8. Effects of process parameters on the morphology of deposits obtained at low current densities. (a) Effect of the concentration of noble metals: 2.5 mA/cm², bath 1 (0.5 mol/L Sn, 0.008 mol/L Ag, and 0.004 mol/L Cu), bath 3 (0.5 mol/L Sn, 0.012 mol/L Ag, and 0.006 mol/L Cu) and bath 4 (0.5 mol/L Sn, 0.024 mol/L Ag, and 0.012 mol/L Cu), 30°C, 0 rpm, and pH 9.5. (b) Effect of bath temperature: 5.0 mA/cm², bath 3 (0.5 mol/L Sn, 0.012 mol/L Ag, and 0.006 mol/L Cu), 0 rpm, and pH 9.5. (c) Effect of agitation. 2.5 and 5.0 mA/cm², bath 3 (0.5 mol/L Sn, 0.012 mol/L Ag, and 0.006 mol/L Cu), room temperature, and pH 9.5. (d) Effect of pH. 2.5 mA/cm², bath 3 (0.5 mol/L Sn, 0.012 mol/L Ag, and 0.006 mol/L Cu), room temperature, and 0 rpm.

(stage 4), the morphology changed to columnar dendrites at 110 mA/cm² and eventually fine dendrites at 120 mA/cm² with severe hydrogen gas evolution. Figure 5 shows the approximated relationship between the polarization curve and surface morphology. The exact boundary between stages was not defined clearly due to the gradual change of morphology with increasing current density. More study will be devoted to defining the exact boundary between stages, especially between stage 1 and stage 2, in the future.

The content of silver and copper, whose deposition potential is higher (less cathodic) than that of tin, tended to drop with increasing current density and is illustrated in Fig. 6. The abrupt drop of the content of noble metals between 10 and 20 mA/cm² is accompanied by the significant change of morphology between two current densities, as shown in Fig. 4. In the case of alloy deposition, the content of each metal in the deposit is thought to be proportional to the partial current (density) induced by the discharge reaction. The absolute partial current density by the discharge of noble metals is constant after the first plateau, but the relative partial current density decreases with increasing current density due to the increase of partial current density by tin discharge. This result indicates that

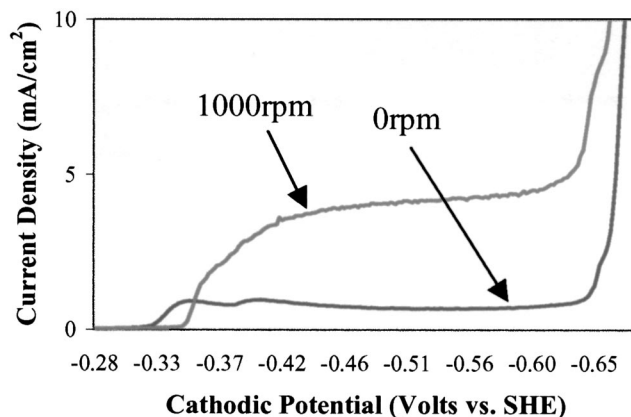


Figure 9. Extension of stage 1 with increasing agitation: 20 mV/s scan rate, bath 6 (0.4 mol/L Sn, 0.01 mol/L Ag, and 0.01 mol/L Cu), room temperature, and pH 9.5.

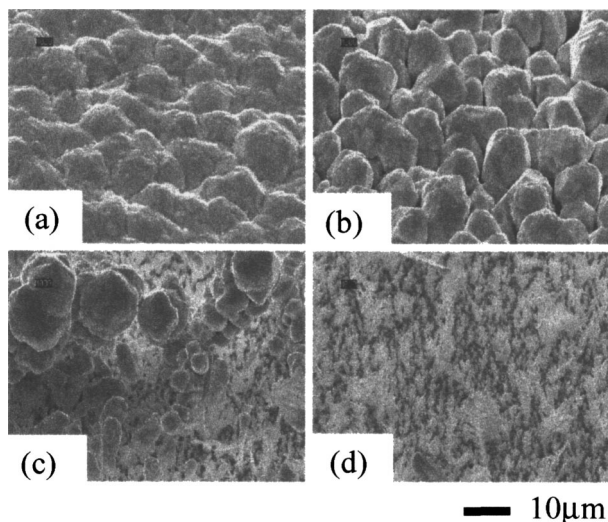


Figure 10. Effect of the ratio of the applied current density (J_a) to the LCD (J_L) on the morphology: (a) $J_a < J_L$, stage 3, (b) $J_a \approx J_L$, stage 4, (c) $J_a > J_L$, stage 4, and (d) $J_a \geq J_L$, stage 4. Bath 1 (0.5 mol/L Sn, 0.008 mol/L Ag, and 0.004 mol/L Cu), room temperature, 0 rpm, and pH 9.5.

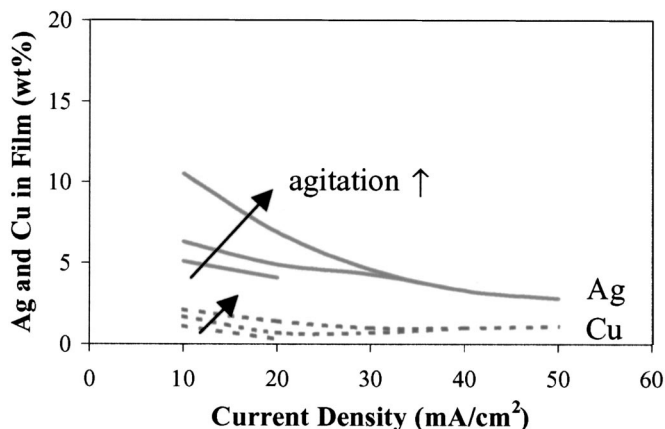


Figure 13. Effect of agitation (0, 100, and 200 rpm) on film composition. Bath 3 (0.5 mol/L Sn, 0.012 mol/L Ag, and 0.006 mol/L Cu), room temperature, and pH 9.5.

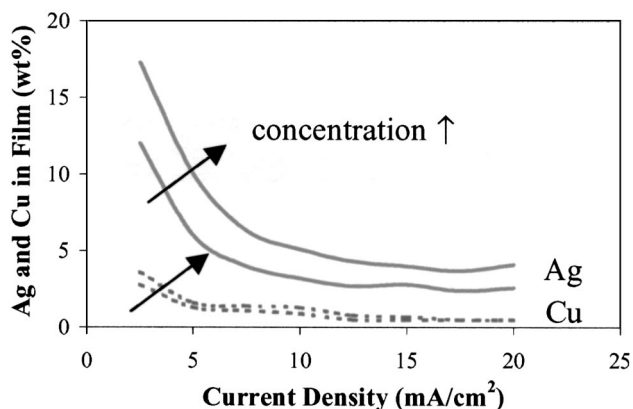


Figure 11. Effect of concentration (bath 1 and 3) of noble metals on film composition. Bath 1 (0.5 mol/L Sn, 0.008 mol/L Ag, and 0.004 mol/L Cu) and bath 3 (0.5 mol/L Sn, 0.012 mol/L Ag, and 0.006 mol/L Cu), room temperature, no agitation, and pH 9.5.

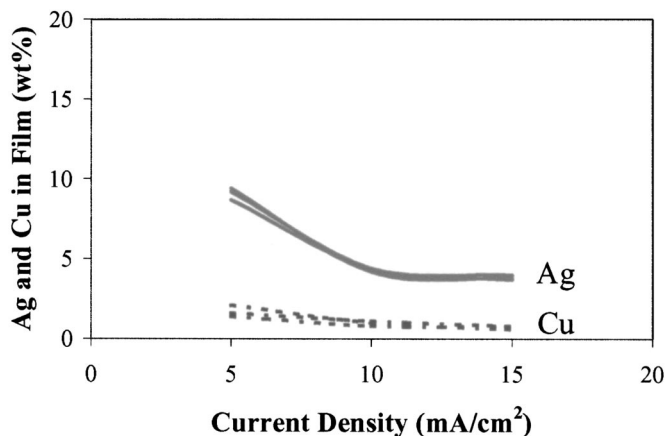


Figure 14. Effect of pH (7.5, 8.5, and 9.5) on film composition. Bath 3 (0.5 mol/L Sn, 0.012 mol/L Ag, and 0.006 mol/L Cu), room temperature, and no agitation.

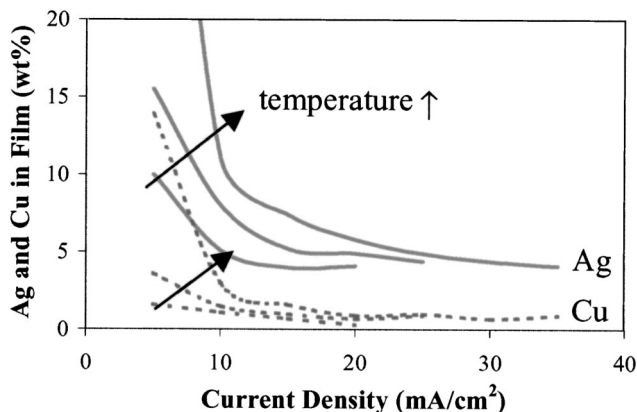


Figure 12. Effect of bath temperature (20, 40, and 50°C) on film composition. Bath 3 (0.5 mol/L Sn, 0.012 mol/L Ag, and 0.006 mol/L Cu), no agitation, and pH 9.5.

Table II. Effects of process parameters on the LCD of ternary alloy deposition (second plateau); conditions in bold increased the LCD.

Parameters	Conditions				LCD (mA/cm ²)
	Bath	Temperature (°C)	Agitation (rpm)	pH	
Base line	3	20	0	9.5	20 (±2.5)
Concentration	5	20	0	9.5	25 (±2.5)
Temperature	3	50	0	9.5	30 (±2.5)
Agitation	3	20	200	9.5	60 (±5.0)
pH	3	20	0	7.5 and 8.5	20 (±2.5)
Combination	5	40	200	9.5	100 (±10)

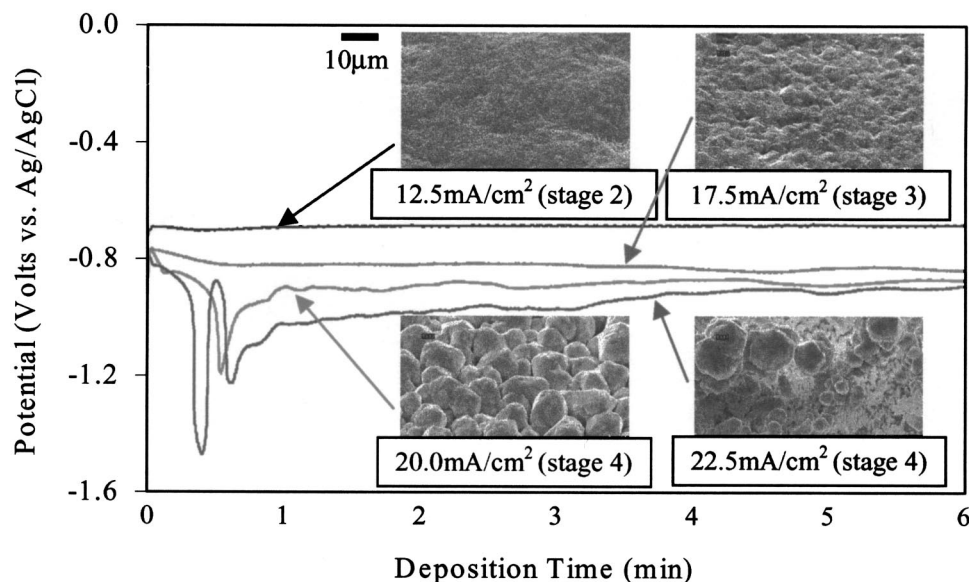


Figure 15. Comparison between chronopotentiometry and surface morphology. Bath 1 (0.5 mol/L Sn, 0.008 mol/L Ag, and 0.004 mol/L Cu), room temperature, no agitation, and pH 9.5.

SnAgCu alloy deposition with this type of bath is of a normal codeposition type.

Effects of process conditions on surface morphology, film composition, and LCD.—Effects of process parameters on the surface morphology of stage 1 and stage 4 were investigated. Most efforts were devoted to evaluating the influence of the concentration of noble metals, bath temperature, and agitation on the morphology of stage 1, based on the assumption that process parameters influencing mass transfer might affect the morphology of stage 1, as these dendrites were caused by the mass-transfer limitation of noble metals. The results were in good agreement with the assumption. Figure 7 shows the experimental results with a conventional RDE, illustrating the change of noble metal LCD with varying process conditions. The LCD of noble metals (first plateau) was increased with increasing the concentration of noble metals, bath temperature, and agitation. It is shown in Fig. 8 that the surface morphology became increasingly dendrite-dominated at a fixed current density with increasing the concentration of noble metals, bath temperature, and agitation. The extension of stage 1 with increasing mass transfer is due to the increase of the noble metal LCD, extending the range at which stage 1 growth was observed. The extension of stage 1 to higher current density with increasing agitation, as an example, is shown in Fig. 9. Accordingly, the shift of stage due to the variation of noble metal LCD can be considered to cause the morphology change at a fixed current density. As can be seen from Fig. 8d, the effect of pH was negligible due to the negligible effect of pH on the noble metal LCD. The morphology of stage 4 was dependent on the ratio of the current density to the LCD and is illustrated in Fig. 10. With increasing the ratio of the applied current density to the LCD, the tip radius of dendrites decreased and the corresponding morphology varied from columnar to finer dendrites due to the increased growth rate. Baths 1-5 all showed the same trend.

Figures 11-14 represent the effect of process conditions on film composition according to the applied current density. The corresponding maximum current density depicted in each figure is close to the corresponding LCD. With increasing the concentration of noble metals (Fig. 11), bath temperature (Fig. 12), and agitation (Fig. 13), the content of noble metals in the film increased. However, the effect of pH was negligible, as can be seen from Fig. 14. That means the deposition of noble metals is under mass-transfer control. An increase in mass transfer increased the LCD of noble metals (first plateau), resulting in the increase of noble metal content in the film at a fixed current density.

A chronopotentiometric method was used to define the LCD of ternary alloy deposition (second plateau) and a comparison was made with the surface morphology. As can be seen from Fig. 15, voltage fluctuation as well as gas evolution was detected along with the columnar growth. More severe fluctuation and gas evolution were associated with finer dendrites. The codeposition of protons is thought to be the source of potential fluctuation. In the case of mass-transfer limitation of metals, the potential drops quickly to proton reduction potential in order to keep the current constant. The LCD of each condition is summarized in Table II. Similar to the results in Fig. 7, the concentration of metal ions (tin in this case), bath temperature, and agitation had a large influence on the LCD. By properly combining those factors, five times higher LCD than that of the baseline was obtained. As expected, the effect of pH was negligible.

Conclusions

A bath and process were developed for dendrite-free, near-eutectic SnAgCu alloy deposition through the investigation of cathodic polarization, morphological transition, and film composition.

Ternary alloys were obtained only when the current density was driven beyond the mass-transfer limitation of noble metals. With increasing current density, the morphological transition occurred through four stages; dendrites, suppression of dendrites, nodules, and columns/dendrites. The content of silver and copper in the film tended to drop with increasing current density.

With increasing the concentration of noble metals, bath temperature, and agitation, the transition current density from stage 1 to stage 2 increased. With increasing the concentration of noble metals, bath temperature, and agitation, the content of noble metals in the film increased at a fixed current density due to an increase in noble metal LCD. The morphology of stage 4 was dependent on the ratio of the applied current density to the LCD, where the LCD of ternary alloy deposition was mainly affected by the concentration of tin ions, bath temperature, and agitation.

Semitoool, Incorporated, assisted in meeting the publication costs of this article.

References

1. T. W. Goodman and E. J. Vardaman, *FCIP and Expanding Markets for Flip Chip*, p. 2, TechSearch International, Inc., TX (1997).
2. P. Elenius and L. Levine, *Chip Scale Rev.*, **2000**, 81 (July/Aug).
3. J. S. Hwang, *Modern Solder Technology for Competitive Electronics Manufacturing*, p. 485, McGraw-Hill, New York (1996).

4. J. F. Ziegler, *IBM J. Res. Dev.*, **40**(1), 3 (1996).
5. S. Arai and T. Watanabe, *Mater. Trans., JIM*, **39**, 439 (1998).
6. H. Shimokawa, T. Soga, T. Nakatsuka, and K. Serizawa, *2001 ICEP Proceedings*, p. 78 (2001).
7. W. Yang, L. E. Felton, and R. W. Messler, Jr., *J. Electron. Mater.*, **24**, 1465 (1995).
8. T. Kobayashi, J. Tanaka, S. Hayashi, T. Takashima, and T. Narita, *2001 ICEP Proceedings*, p. 66 (2001).
9. W. K. Choi and H. M. Lee, *J. Electron. Mater.*, **29**, 1207 (2000).
10. S. Chada, R. A. Fournelle, W. Laub, and D. Shangguan, *J. Electron. Mater.*, **29**, 1214 (2000).
11. C. Tanner, *International Workshop on Lead- and Halide-free Electronics*, Semicon Europa, Paper K (2000).
12. K. Nimmo, *International Workshop on Lead- and Halide-free Electronics*, Semicon Europa, Paper E (2000).
13. I. Ohnuma, M. Miyashita, K. Anzai, X. J. Liu, H. Ohtani, R. Kainuma, and K. Ishida, *J. Electron. Mater.*, **29**, 1137 (2000).
14. M. Miyazaki, K. Oki, S. Nomura, T. Takei, N. Katayama, H. Tanaka, and M. Akanuma, *2001 ICEP Proceedings*, p. 60 (2001).
15. M. Kitajima, T. Shono, M. Takesue, M. Noguchi, and K. Yamazaki, *2001 ICEP Proceedings*, p. 72 (2001).
16. K. Suganuma, *International Workshop on Lead- and Halide-free Electronics*, Semicon Europa, Paper B (2000).
17. I. E. Anderson, F. G. Yost, J. F. Smith, C. M. Miller, and R. L. Terpstra, U.S. Pat. 5,527,628 (1996).
18. S. G. Gonya, J. K. Lake, R. C. Long, and R. N. Wild, U.S. Pat. 5,393,489 (1995).
19. M. R. Paruchuri and D. Shangguan, U.S. Pat. 5,833,921 (1998).
20. G. Solomon, *TAP Technology*, **29** (2001).
21. L. Graham, Ph.D. Thesis, p. 41, Rensselaer Polytechnic Institute, Troy, NY (2000).